


## Article

# Influence of Piloti Forms on Wind Comfort of Different Building Group Layouts by Large Eddy Simulation

Yueyun Hu<sup>1</sup>, Congchuan Hu<sup>2</sup>, Guangdong Liu<sup>2</sup>, Xiaofang Shan<sup>1,3</sup>, Qinli Deng<sup>1,3,\*</sup> , Zhigang Ren<sup>1,3</sup> and Qianyu Tang<sup>4</sup>

<sup>1</sup> School of Civil Engineering and Architecture, Wuhan University of Technology, Wuhan 430070, China

<sup>2</sup> Luneng Group Co., Ltd., No. 5 Chaowai Street, Chaoyang District, Beijing 100023, China

<sup>3</sup> Hainan Institute, Wuhan University of Technology, Sanya 572000, China

<sup>4</sup> Building Energy Research Center, Tsinghua University, Beijing 100084, China

\* Correspondence: deng4213@whut.edu.cn; Tel.: +86-27-87651786

**Abstract:** This paper studies the influence of different piloti rates (0%, 20%, 40%, 60%, 80%, 100%) on outdoor wind comfort for three building groups, i.e., determinant type, point type, and enclosure type. LES (Large Eddy Simulation) is used to simulate the wind environment of three clusters at six different piloti rates. This paper mainly studies the effect of piloti rate on wind speed at pedestrian level (1.5 m). The outdoor wind environment was analyzed using the average wind speed ratio, and outdoor wind comfort was evaluated using the comfortable wind ratio. The following results were obtained: (1) The piloti setting has little influence on the overall wind speed in the target area, and even an inappropriate piloti rate setting may reduce the overall average wind speed in the target area. (2) A comprehensive comparison of the three building layouts shows that the comfortable wind ratio of the determinant layout is the highest when the piloti ratio is 80%. The results of this study can provide architects and urban planners with reference for piloti and urban layout settings.

**Keywords:** outdoor wind environment; wind comfort; urban form; large eddy simulation; piloti rate



**Citation:** Hu, Y.; Hu, C.; Liu, G.; Shan, X.; Deng, Q.; Ren, Z.; Tang, Q. Influence of Piloti Forms on Wind Comfort of Different Building Group Layouts by Large Eddy Simulation. *Buildings* **2023**, *13*, 234. <https://doi.org/10.3390/buildings13010234>

Academic Editor: Francesco Ricciardelli

Received: 9 December 2022

Revised: 6 January 2023

Accepted: 11 January 2023

Published: 13 January 2023



**Copyright:** © 2023 by the authors. Licensee MDPI, Basel, Switzerland. This article is an open access article distributed under the terms and conditions of the Creative Commons Attribution (CC BY) license (<https://creativecommons.org/licenses/by/4.0/>).

## 1. Introduction

The safety and comfort of pedestrians around urban buildings largely depend on the wind environment at the height of the pedestrian floor [1–4]. In order to solve this problem, people have done a lot of research on pedestrian wind environments [5–9]. To clarify what urban layout, building shape, vegetation, building density, and other factors can make the wind environment of the pedestrian floor safe and comfortable [10–12]. Therefore, it is of great significance for architectural designers and decision makers to improve pedestrian level wind environment and create good pedestrian wind comfort.

In recent years, in order to improve the wind environment at urban pedestrian levels and enhance the comfort of the wind environment, people have adopted some strategies [13–16].

Cui [17] quantitatively evaluated the pedestrian wind environment of a U-shaped canyon by conducting particle image test experiments in wind tunnels. The results show that the wind speed of a U-shaped canyon at pedestrian height is generally lower than that of a parallel canyon, especially in a parallel wind direction. Weerasuriya [18] tested the influence of twisted wind characteristics on pedestrian altitude wind speed in a boundary layer wind tunnel. Taking Tsuen Wan, Hong Kong, as the research object, we found that the wind speed of the twisted wind largely depends on the size and direction of the yaw angle; especially in nearby areas with low densities of buildings, the local wind circulation is significantly affected by the twisted wind. Through a wind tunnel experiment, He [19] studied the influence of irregularity (fragmentation, angularity, and curvature) and permeability on the wind environment of the pedestrian floor. The results show that the wind environment at pedestrian level is negatively correlated with urban irregularity. There is a

positive correlation between the wind performance of the pedestrian layer and urban permeability. Ikegaya [20] used the computational fluid dynamics (CFD) method to study the wind field of the pedestrian floor around the building with an aspect ratio of 1:1:2. It is proposed that the evaluation method of peak factor can better evaluate the wind environment on a pedestrian floor.

Piloti design plays a huge role in improving the microclimate around buildings [21]. In hot summers, a piloti design can not only provide shade for people but also improve the ventilation effect around the building [22]. Du [23] studied the shapes of “I”, “L”, “U”, and “□” of four common building structures through CFD, used the average wind speed ratio and the average wind speed change rate to identify wind comfort, and quantitatively evaluated the improvement brought by the “lift-up” design. The results show that the piloti design can improve the wind comfort of the built environment, and its influence degree is closely related to the incident wind direction. Among them, the wind comfort under the oblique wind direction is better than the other two wind directions. Huang [24] compared the differences in meteorological parameters and response heat perception between the piloti part of the piloti building and the area directly exposed to outdoor sunlight based on field measurement and subject questionnaire. The results show that most people report feeling more comfortable in the shade of a piloti building. Meanwhile, through data analysis, it is concluded that solar radiation and wind speed are the two main factors affecting outdoor thermal comfort. Sha [25] used CFD to study the influence of piloti design with different wind directions on pedestrian wind comfort. The results show that when the wind direction is between 30° and 45°, the open-air setting is more effective reducing the concentration of pollutants than at 0° and 15°. The piloti design can enhance the dilution of pollutant concentrations in all winds. Tse [26] studied the influence of piloti design and size on the surrounding wind environment through a wind tunnel experiment. The results show that the piloti height is the parameter that has the greatest influence on the surrounding wind environment. Chen [27] used the CFD method to explore the impact of building height and upstream buildings on piloti buildings. The results show that the piloti building is taller or shorter than the upstream building, which can make the surrounding wind environment better. However, increasing building height and removing upstream buildings are not necessarily beneficial to the surrounding wind environment of the piloti buildings.

Computational wind engineering simulation research originated around 1963, when Smagorinsky [28] developed one of the first successful LES methods. With the improvement of computing power, large eddy simulation is becoming more and more popular in wind engineering. Muralam [29] and Yu Da-Hai [30] applied the LES model to study the flow around the blunt body. The results show that although the LES model can accurately reflect the complex characteristics of flow around a blunt body, it is difficult to apply in engineering due to the large amount of calculation. Shah KB [31] found that LES could well predict the phenomenon of flow around blunt bodies and provide important information for wind engineering researchers. Selvan [32] used the LES model to study the full-scale wind tunnel experiment, and the results showed that the prediction of the mean value was in good agreement with the measured results. Kravchenko AG [33] studied the large-eddy numerical simulation of subcritical flow around a cylinder and proposed some key problems to appropriately simulate the numerical simulation of flow around a blunt body. Tutar [34] used large eddy simulation to conduct a numerical study on two parallel buildings and presented the distribution characteristics of the flow field of the parallel buildings. Lim HC [35] used LES to study a rectangular building located in a turbulent boundary layer, and the results showed that a reasonable incoming flow and computational domain boundary can greatly improve the coincidence between LES and test results. In general, LES performs better than other turbulence modeling methods but requires much more computing resources.

Existing wind environment studies are mainly focused on the layout of buildings without piloti or with the piloti wind environment of a single building or a row of buildings.

It is generally ignored that the diverse and complex forms of urban blocks will increase the uncertainty of the effect of piloti design on improving the wind environment. In addition, there is a lack of research on the wind comfort of pedestrian floors based on the building overhead rate in urban blocks. This study considers the complexity of the form of urban blocks, and the target area of the study is set in the middle of the architectural complex. At the same time, this study is not conducted on a single building or a single row of buildings but on a small group of buildings so as to ensure the credibility of the research results. In this study, six different overhead rates were set up to study the influence of different piloti rates on the surrounding wind environment, and it was found that the piloti rate was the best for pedestrian wind comfort. At the same time, three commonly used building layouts are selected, and the comparison between these three building layouts is also made, and it is obtained that the building layout has the best piloti rate and pedestrian wind comfort. This study provides some suggestions for urban planners to mitigate the increasingly serious urban heat island effect.

## 2. Methodology

### 2.1. CFD Turbulence Models

The 3D Navier-Stokes (NS) equation is used for flow computations. The technique of LES with the Smagorinsky model is used for turbulence modeling. The continuity and momentum equations in tensorial notation are as follows:

Continuity Equation:

$$\frac{\partial \bar{U}_i}{\partial X_i} = 0 \quad (1)$$

Momentum Equation:

$$\frac{\partial \bar{U}_i}{\partial t} + \frac{\partial \bar{U}_i \bar{U}_j}{\partial X_j} = -\frac{\partial \bar{P}}{\partial X_j} + 2 \frac{\partial}{\partial X_i} (\nu + \nu_{sgs}) \bar{S}_{ij} \quad (2)$$

The variable ‘ $\nu$ ’ in Equation (2) is the kinematic viscosity of fluid, whereas ‘ $\nu_{sgs}$ ’ is the turbulent kinematic viscosity given as:

$$\nu_{sgs} = (C_s \Delta)^2 \sqrt{2 \bar{S}_{ij} \bar{S}_{ij}} \quad (3)$$

‘ $C_s$ ’ is the Smagorinsky constant taken as  $C_{sgs} = 0.167$  for the current work, and ‘ $\Delta$ ’ is the cube root of the volume of a cell used in the Smagorinsky model, which is given as:

$$\Delta = \sqrt[3]{\Delta x \Delta y \Delta z} \quad (4)$$

Similarly,  $\bar{S}_{ij}$  in Equation (2), the shear rate tensor computed as:

$$\bar{S}_{ij} = \frac{1}{2} \left( \frac{\partial \bar{U}_i}{\partial X_j} + \frac{\partial \bar{U}_j}{\partial X_i} \right) \quad (5)$$

### 2.2. Assessment Approach

#### 2.2.1. Mean Wind Speed Ratio

In this study, the average wind speed was used to evaluate the outdoor wind environment and wind comfort. In order to make the study more general, the normalized average wind speed is used in this study. The mean velocity ratio (MVR) is calculated as follows.

$$MVR = \frac{U_N}{U_{ref}} \quad (6)$$

where,  $U_N$  is the average wind speed at any point on the pedestrian floor,  $U_{ref}$  is the average wind speed at the entrance height of 1.5 m,  $U_{ref} = 1.528$  m/s.

### 2.2.2. Comfortable Wind Ratio

In this study, the comfortable wind ratio was used as the evaluation standard for outdoor comfortable wind. The so-called comfortable wind ratio refers to the area occupied by the comfortable wind in the target area over the area of the target area. However, because the area occupied by comfortable wind is not easy to calculate, a point selection process is carried out for the target area. Therefore, the comfortable wind ratio in this study is the ratio of the number of points in the comfortable wind speed interval of the target area to the total number of points in the target area.

### 2.2.3. Outdoor Comfortable Wind Evaluation Criteria

The influence of outdoor wind environments on human wind perception is mainly manifested in two aspects: the influence of wind on human behavior and the influence of wind on human thermal comfort. Wind speed and the fluctuation of wind speed are the key factors affecting people's feeling of wind, but the ambient air temperature, humidity, people's clothes, and solar radiation factors also affect people's feeling of wind. Taking all the factors into consideration will be a very complicated problem. Many international studies have proposed the upper limit of wind speed from the perspective of human behavior safety, but this method can only evaluate the uncomfortable problems caused by strong winds, and few studies have defined the wind speed range in terms of thermal comfort. In 1985, according to the influence of temperature on wind perception, Japanese scholars Yasunari Murakawa and Yasunari Morikawa proposed the evaluation criteria for wind speed from the perspectives of safety and comfort [36], as shown in Table 1.

**Table 1.** Evaluation principle of velocity considering temperature influence.

Evaluation Range	Temperature Range (°C)		
	<10	10~25	>25
Range of breezes that cause thermal discomfort in the human body (m/s)	—	—	<0.7
Human comfortable wind speed range (m/s)	<1.3	<1.5	0.7~1.7
Excessive range between comfortable and uncomfortable winds (m/s)	1.3~2.0	1.5~2.3	1.7~2.9
Range of strong winds that cause human discomfort (m/s)	>2.0	>2.3	>2.9

## 2.3. Turbulence Model Validation

### 2.3.1. Case Description

The experimental data for wind field turbulence model validation in this study refers to the wind tunnel test of the Japan Building Association AIJ [37]. As shown in Figure 1a, the cube represents a single building, and its size is 0.2 m ( $D_1$ )  $\times$  0.2 m ( $W_1$ )  $\times$  0.2 m ( $H$ ). Figure 1b shows the 120 measurement points in the X-Y plane. Based on these 120 points, the simulation results are compared with experimental data, and the correlation coefficient is obtained.

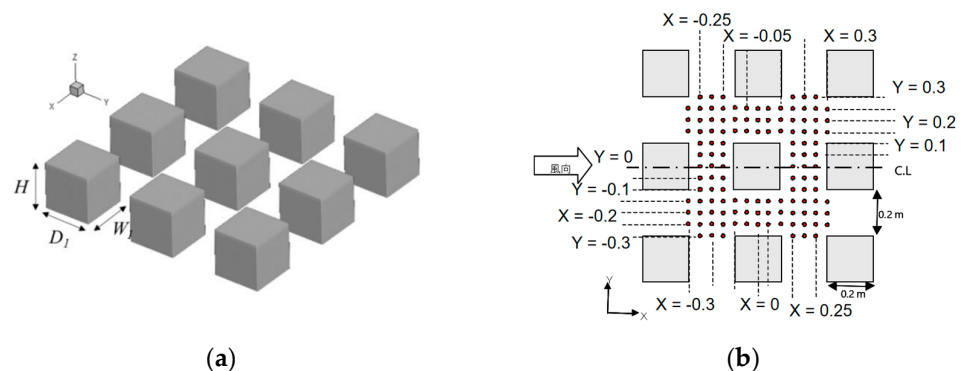


**Figure 1.** Wind tunnel model and schematic diagram of measuring points. (a) A wind tunnel experimental physical model. (b) Measuring point azimuth diagram.

As recommended by the Japanese AIJ guide, the computational domain entrance is 5H away from the windward section of the building (H is the height of the building, which is 0.2 m in this model), and the boundary of the computational domain on both sides is 5H away from the building. The top computing domain boundary is 10H away from the building, and the outlet boundary computing domain is 15H away from the rear end of the leeward building. The blocking rate for this arrangement is 1.8%.

### 2.3.2. Boundary Conditions

The inlet boundary condition is the exponential rate function obtained by fitting the experimental data measured in the wind tunnel experiment, and the equation of the inlet wind speed is  $\frac{u_z}{u_H} = \left(\frac{Z}{H}\right)^\alpha$ , where  $u_H$  is the reference wind speed at the building height ( $Z = 0.2$  m),  $u_H = 3.654$  m/s;  $u_z$  is the wind speed at the entrance  $Z$  height;  $\alpha$  is ground roughness,  $\alpha = 0.28$ .

### 2.3.3. Wind Environment Verification Result

Two lines,  $x = -0.25$  m and  $y = 0.25$  m, were selected for comparison and verification between simulated data and wind tunnel tests. The verification results are shown in Figure 2. In Figure 2, the y-axis is the wind speed ratio, and the x-axis is the coordinate of the layout of measuring points in Figure 1b. For the line  $x = -0.25$  m, the coordinate on the x-axis in Figure 2a is the coordinate point of  $y$  in Figure 1b. For the line  $y = 0.25$  m, the coordinate on the x-axis in Figure 2b is the coordinate point of  $x$  in Figure 1b. When  $x = -0.25$  m, the Spearman correlation is 0.929 and the confidence level is 99%. While  $y = 0.25$  m, the M-S Spielman correlation was 0.912, with a significance level of 99%. Therefore, the simulation results can be considered credible.

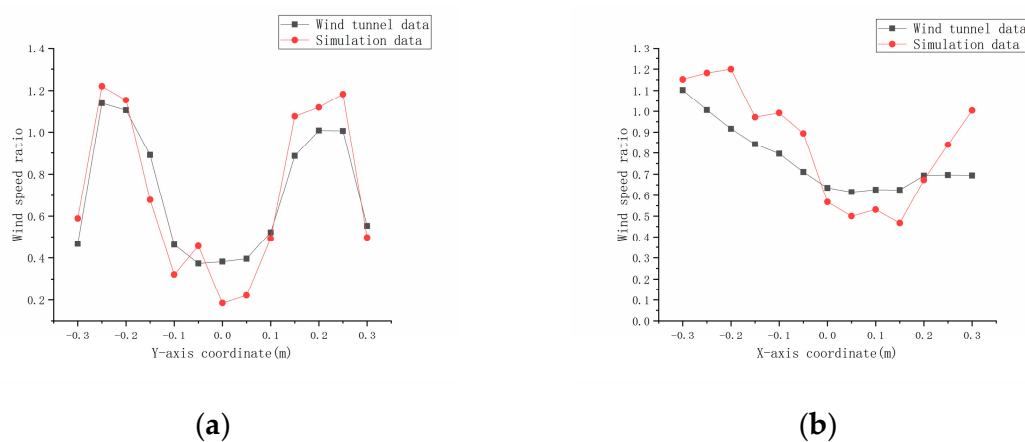


**Figure 2.** Comparison between wind tunnel and simulated data. (a) Location of the county:  $x = -0.25$  m. (b) Location of the county:  $y = 0.25$  m.

## 3. Building Configuration Description

### 3.1. Building Configuration

The analytical model in this study is determined by referring to three common residential layouts, i.e., determinant cluster, point cluster, and enclosing cluster, in Wuhan, China.

As shown in Figure 3, the architectural complex designed by this research institute consists of 88 single buildings in 8 rows and 11 columns. The size of the computational domain is  $1882 \times 1204 \times 462$  m, and the design size of the entire architectural complex is  $1000 \times 700$  m. The distance between the front, left, and right of the entire building complex and the edge of the computing domain is 252 m ( $6H$ ,  $H = 42$  m), and the distance between the rear and the edge of the computing domain is 630 m ( $15H$ ), which is in line with the recommended setting in the AIJ guide. The maximum blocking rate of the model in this study is 3.6%, which is slightly higher than the 3% blocking rate recommended by

the guideline, but as long as the blocking rate is less than 10% [38], the result can also be considered reliable.

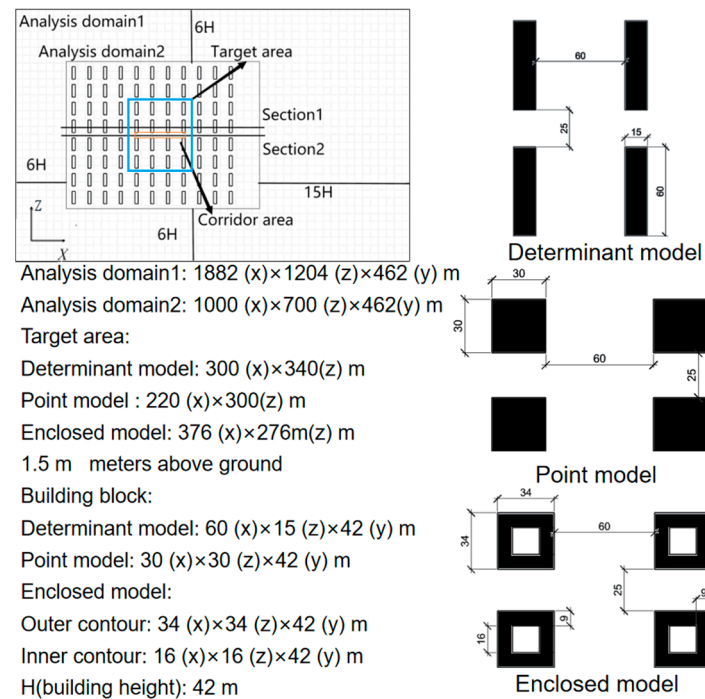


**Figure 3.** Architectural layout diagram.

The dimensions of a single building are shown in Figure 3. The distance between the front and back of the building is 60 m, and the distance between the left and right sides of the building is 25 m. The building size of the determinant group was 60 m (x) × 15 m (z) × 42 m (y); the point group building size was 30 m (x) × 30 m (z) × 42 m (y). The dimensions of the surrounding building are 34 m (x) × 34 m (z) × 42 m (y), and the dimensions of the inner building are 16 m (x) × 16 m (z) × 42 m (y). Although each model is different in size, its footprint is the same.

In order to eliminate the uncertainty of wind environment effect of piloti design in complex urban blocks, 16 single buildings in the center of an architectural complex were selected as the target area. The target areas of determinant, point, and enclosed types are 300 × 340 m, 220 × 300 m, and 376 × 236 m, respectively. Although the target area is different in size, its position in the whole building group is the same. There are four rows of buildings in the front row, three rows of buildings in the back row, and two rows of buildings on the left and right. At the same time, the pedestrian height of the middle passage and piloti area in the target area are studied separately. In order to study the direction of the wind in the target area, the vector diagrams of the middle section of the target area and the middle section of the building in the target area are studied. As shown in Figure 3, the middle section of the target area is Section 1. The middle section of the building in the target area is Section 2. For the determinant model, point model, and enclosed model, Section 1 is the Z = 602 m section, and Section 2 are Z = 644.5 m, Z = 629.5 m, and Z = 631.5 m, respectively.

Table 2 shows the introduction to each case. The piloti rate of each model is 0%, 20%, 40%, 60%, 80%, and 100%. The area of different groups in this study is the same. The piloti form studied is that the piloti part begins in the middle and gradually spreads to both sides. As shown in Table 1, the so-called piloti ratio is the ratio of the horizontal area of 3 m of the building to the floor area of the building. As shown in Figure 4, the so-called piloti area refers to the part of the building raised from the ground to allow the air to flow through.

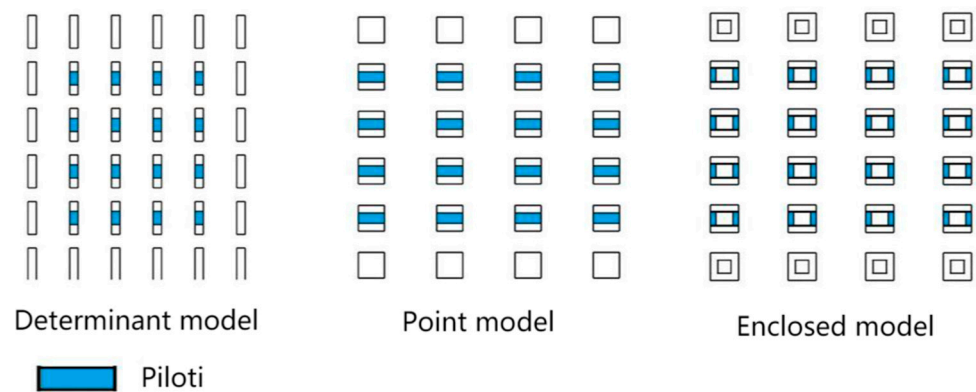


**Figure 4.** Building model piloti diagram.

**Table 2.** Analysis cases.

Case	Floor Space (m <sup>2</sup> )	Model	Piloti Ratio	Piloti Area (m <sup>2</sup> )
case1	900	Determinant	0%	0
case2	900	Determinant	20%	180
case3	900	Determinant	40%	360
case4	900	Determinant	60%	540
case5	900	Determinant	80%	720
case6	900	Determinant	100%	900
case7	900	Point	0%	0
case8	900	Point	20%	180
case9	900	Point	40%	360
case10	900	Point	60%	540
case11	900	Point	80%	720
case12	900	Point	100%	900
case13	900	Enclosed	0%	0
case14	900	Enclosed	20%	180
case15	900	Enclosed	40%	360
case16	900	Enclosed	60%	540
case17	900	Enclosed	80%	720
case18	900	Enclosed	100%	900

### 3.2. Boundary Condition

The software used in this study is Openfoam-v8.

The boundary condition type of inlet velocity is codeFixedValue, and the power law air inlet velocity is adopted. The formula is  $U = U_5 \left( \frac{Z}{Z_5} \right)^\alpha$ , where  $U_5$  is the summer wind speed in Wuhan, China [39],  $U_5 = 2.7$  m/s,  $Z_5 = 10$  m, and the ground roughness  $\alpha$  is set to 0.3. The exit boundary condition is pressureInletOutletValue. The wall boundary condition is set to noSlip. The inlet flow set is a laminar flow inlet.

The pressure boundary condition type for the entrance and wall is set to zeroGradient. The outlet boundary condition type is set to totalPressure, which corresponds to the velocity in the inlet boundary condition.

The viscosity boundary conditions of the inlet, outlet, and wall are type calculated.

The total calculation time step is 1200 s. 1200 s is calculated from the inlet wind speed blowing across the entire computing domain to allow adequate fluid development. At the same time, the number of co was set, the maximum set is not more than 1.

The time term of the NS equation is approximated using the Euler difference scheme, while the convection, gradient, and LaPlace terms are approximated using Gauss linear approximations. The precision of the solution of the NS equation is  $10^{-6}$ .

The turbulence condition used in this paper is  $I(Z) = 0.1 \left( \frac{Z}{Z_s} \right)^{-\alpha-0.05}$ , where  $\alpha = 0.3$ ,  $Z_s = 462$  m, and  $Z$  is the height.

### 3.3. Grid Introduction

Figures 5 and 6 show the grid picture of the x-y and x-z sections when the piloti ratio of the determinant model is 0%. The author densified the target area studied and adopted a relatively sparse grid layout far away from the building model. The boundary layer grid of the first floor of the buildings in the target area is  $1.6 \times 10^{-3}$  ( $y+ < 8$ ). The grid number of all models is shown in Table 3.

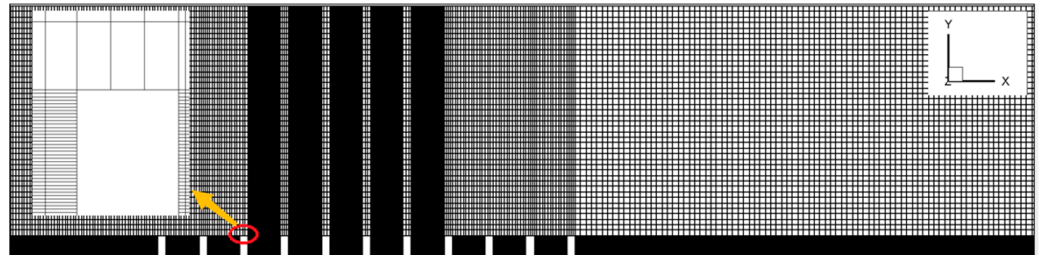


Figure 5. Schematic diagram of the x-y section grid.

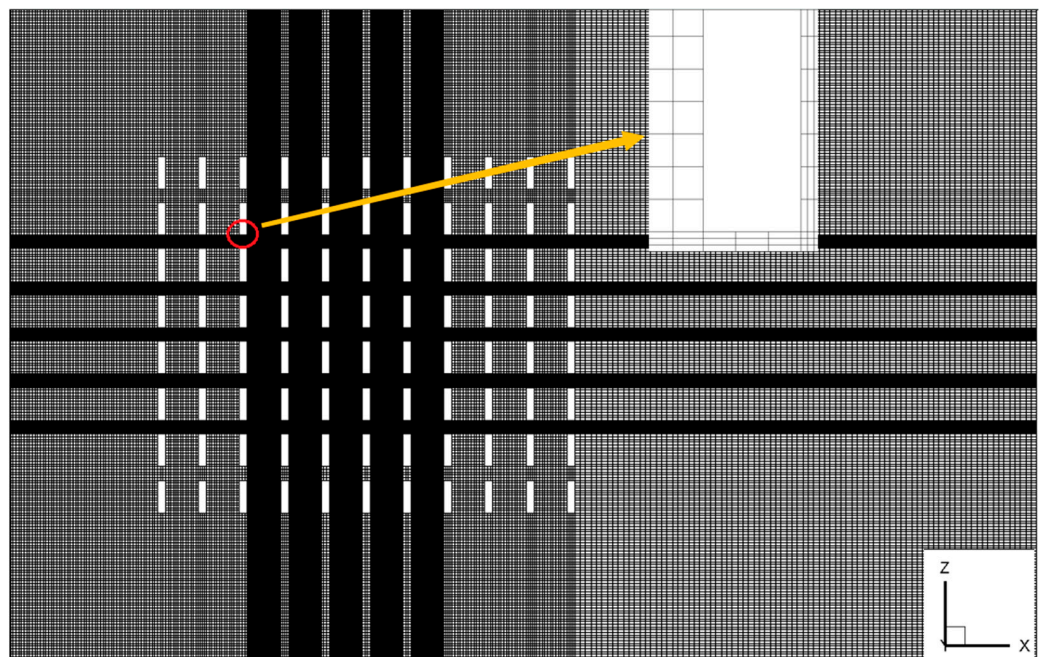


Figure 6. Schematic diagram of the x-z section grid.

Table 3. Grid information.

Piloti Rate	0%	20%	40%	60%	80%	100%
Grid number of the determinant model ( $10^4$ )	2304	1607	1600	1625	1625	1597
Grid number of the point model ( $10^4$ )	2305	1671	1653	1668	1671	1644
Grid number of the enclosed model ( $10^4$ )	2306	1715	1746	1752	1749	1715



## 4. Results and Discussion

### 4.1. The Effects of Piloti Design in the Determinant Group

#### 4.1.1. The Effects of Piloti Design on Pedestrian Layer Wind Speed in the Target Area

As shown in Figure 7, the overall average wind speed ratio of target areas with different piloti rates presents a downward trend as a whole, with slight, but small, fluctuations in the middle. When the piloti ratio is 100%, the reason why the average wind speed ratio suddenly rises is that there are no obstacles at the bottom, which leads to the increase of the average wind speed ratio. Therefore, for the determinant model, the increase in piloti rate has a negative effect on the average wind speed of pedestrian height in the target area.

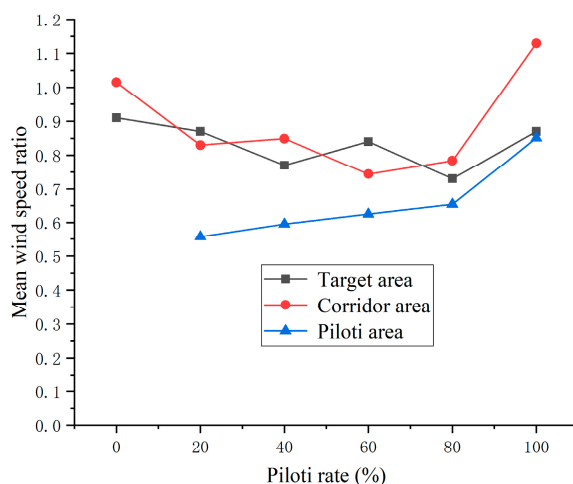


**Figure 7.** Variation of the mean wind speed ratio in the determinant model.

Combined with Figures 8 and 9, it can be known that the mainstream wind speed in the target area is countercurrent wind. The regional average wind speed ratio does not increase with the increase of the building piloti rate because the target area is located in the middle part of the building complex and there are obstacles in front of it. Therefore, when the wind blows into the target area, the wind speed in the target area has been attenuated, so the wind speed in the target area is small. However, there are no obstacles around the whole building complex, so the wind speed is relatively high. In the target area of the building complex, the wind speed outside the building complex is large while the wind speed in the target area is small, so the wind outside the building complex will flow to the inside of the building complex, and the inside of the target area is affected by the side wind. Furthermore, as shown in Figure 8, when the side wind enters, the wind direction from the side changes from the downwind direction to the opposite wind direction due to the obstruction of buildings. In the target area, the wind speed of the countercurrent wind is higher than that of the downcurrent wind, so most of the wind direction in the target area changes.

#### 4.1.2. The Effects of Piloti Design on the Wind Speed at the Pedestrian Level of the Aisle in the Target Area

As shown in Figure 7, the average pedestrian wind speed ratio in the middle aisle of the target area generally presents a downward trend. Combined with Figure 10, it can be seen that the dominant wind in the middle corridor of the target area is countercurrent wind, while some wind direction blows upward, resulting in the decline of wind speed on the pedestrian floor. When the piloti ratio is 100%, the increase in the average wind speed ratio is due to the fact that there is no obstacle to block it, which leads to the increase in the average wind speed.

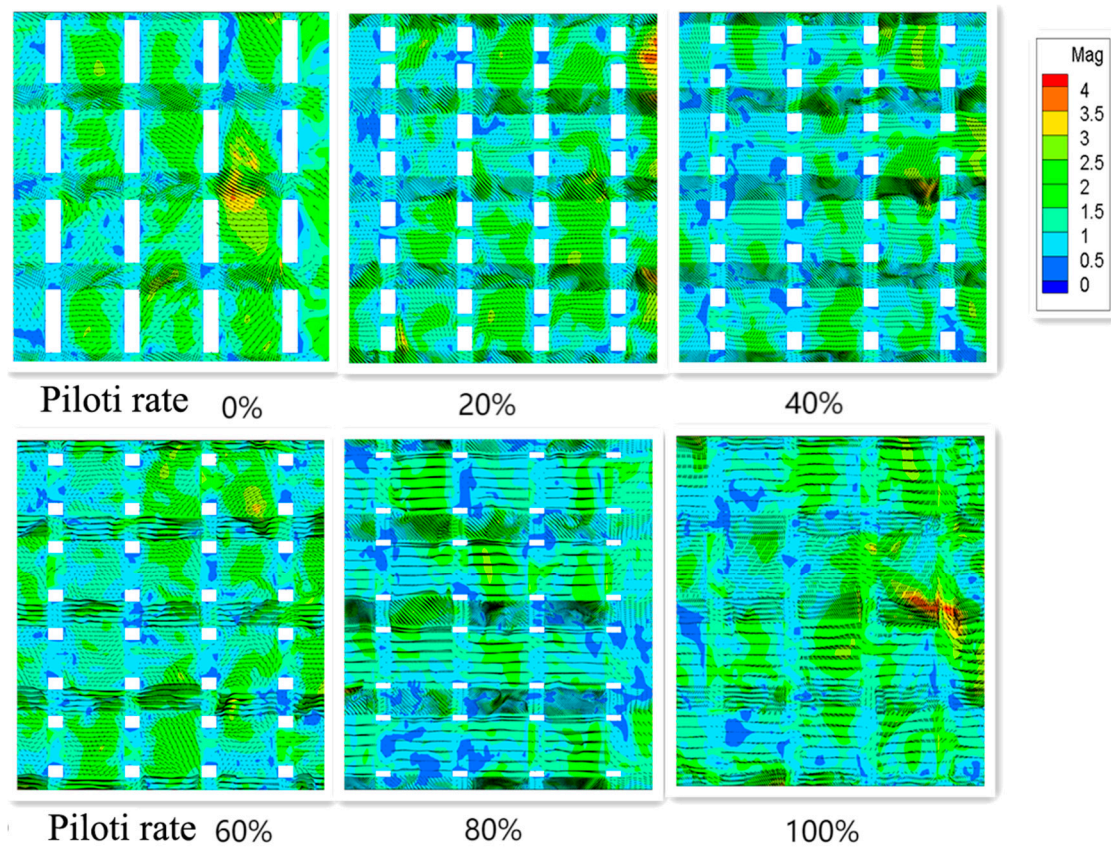


Figure 8. Vector diagram of the target area of a pedestrian layer.

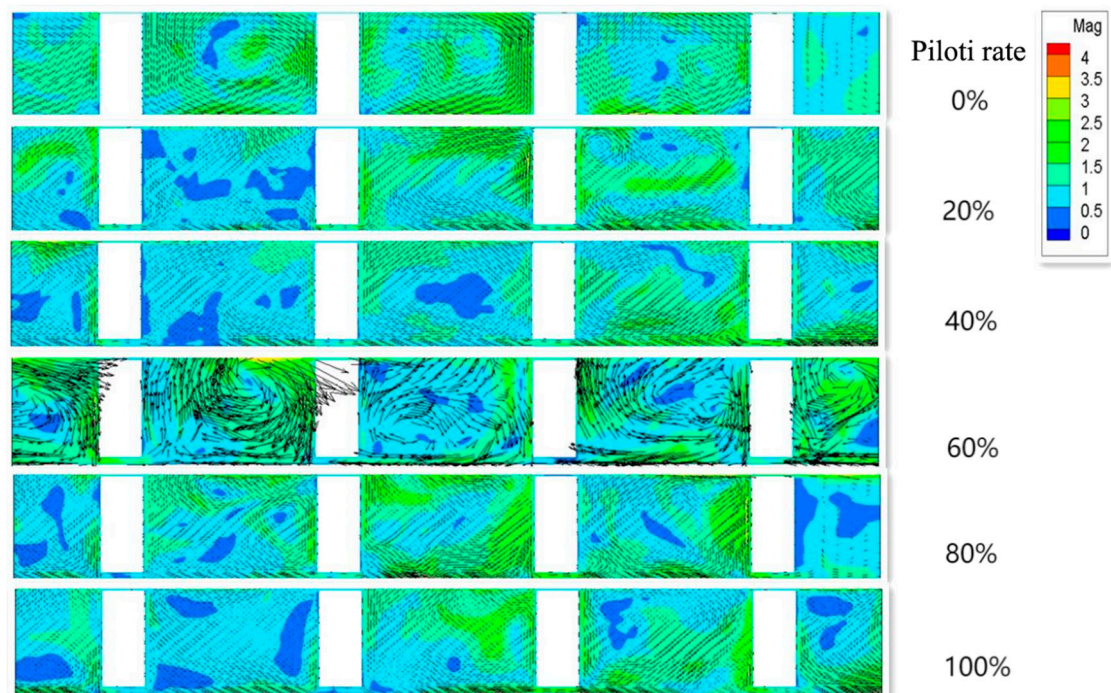
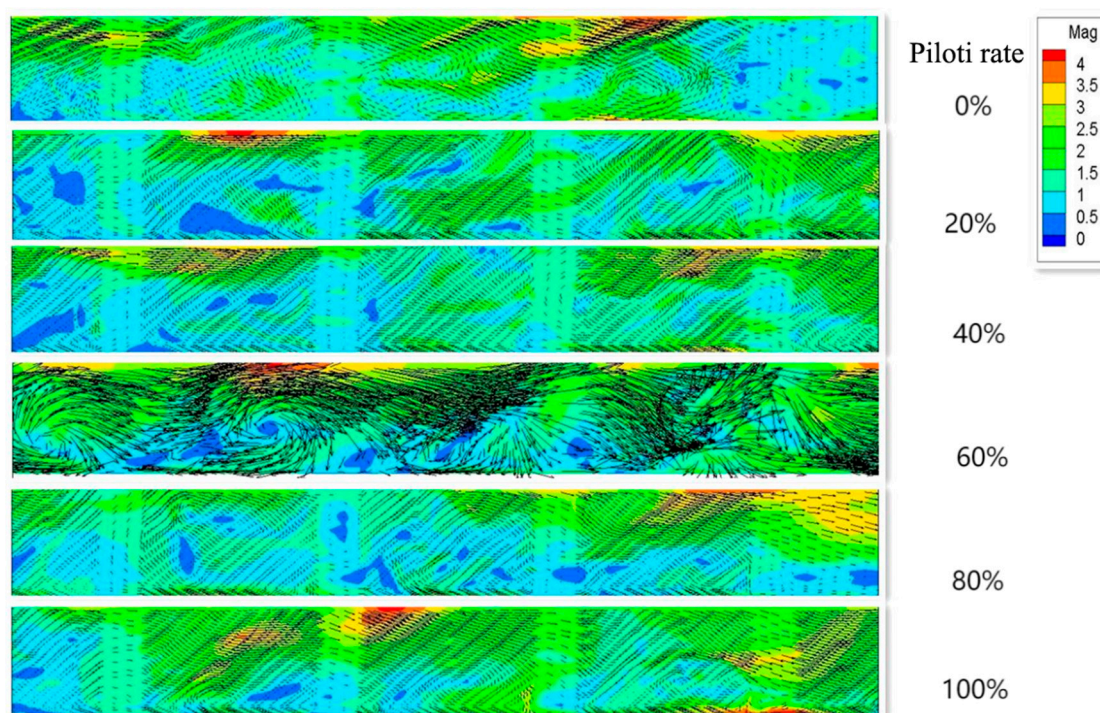


Figure 9. Vector diagram of the target area of Section 1 (Determinant model).



**Figure 10.** Vector diagram of the target area of Section 2 (Determinant model).

#### 4.1.3. The Effects of Piloti Design on Wind Speed of the Pedestrian Layer in the Piloti Area

As shown in Figure 7, with the increase in piloti rate, the average wind speed ratio of the pedestrian floor height in piloti areas also gradually increases. It is highest when the piloti rate is 100% because it is fully piloti and there is no obstruction because the average wind speed is at a maximum. Therefore, for the determinant model, the increase in the piloti rate can increase the average wind speed of pedestrian height in the piloti space.

#### 4.1.4. The Effects of Piloti Design on Pedestrian Layer Wind Comfort in the Target Area

The hottest month in Wuhan is July, with an average temperature of 28.4 °C [39]. Therefore, its comfortable wind range is 0.7–1.7 m/s.

The target area of the study was sampled every 0.5 m, and 355,705, 368,105, 380,009, 391,913, 403,817, and 415,721 points were selected for the piloti rate ranging from 0% to 100%.

The bar chart of the ratio and number of comfortable wind points on pedestrian floors with different piloti rates in the target area is shown below. It has been discovered that, in the target area, the proportion of comfortable wind increases as the piloti rate increases. However, when the piloti rate is 100%, the proportion of large wind speeds increases, leading to a decline in the comfortable wind ratio.

At the same time, it can be seen from Figure 11 that when the piloti rate increases from 0% to 20%, the comfortable wind ratio increases by 1.66%, with a small increase in the ratio range. However, from 20 to 40 percent, the comfortable wind ratio increased significantly, by 4.96 percent. From 40% to 60% and from 60% to 80%, the comfortable wind ratio increased by 1.76% and 1.04%, respectively.

Therefore, it can be concluded that in the summer, for the determinant group, the comfortable wind ratio increases with an increase in the piloti rate, but if the piloti rate exceeds 80%, because of the increase in the large wind speed, the comfortable wind ratio decreases. At the same time, it can be concluded that when the piloti rate is between 20% to 40%, the comfortable wind ratio increases the most.

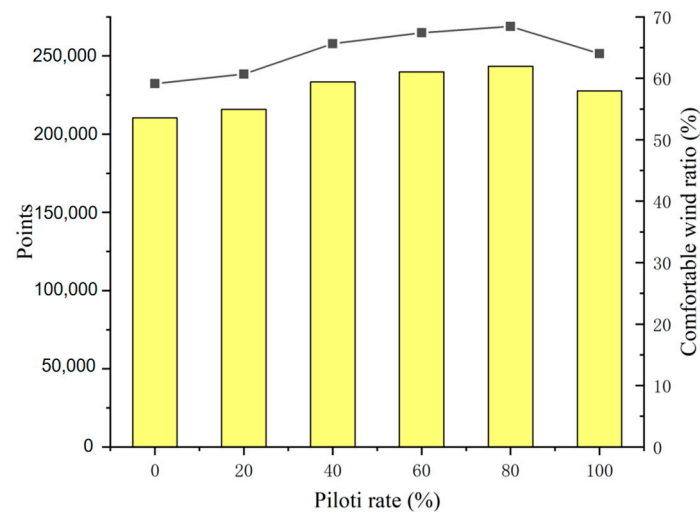


**Figure 11.** The changing pattern of a comfortable wind ratio under different piloti rates (Determinant model).

#### 4.2. The Effects of Piloti Design in the Point Group

##### 4.2.1. The Effects of Piloti Design on Pedestrian Layer Wind Speed in the Target Area

It can be seen from Figure 12 that the overall wind speed ratio of target areas under different piloti rates fluctuates, but the fluctuation is small. The maximum difference between two piloti rates does not exceed 0.07 except when the piloti rate is 100%. The maximum wind speed ratio occurs on layouts with a 100% piloti ratio, but this is because there are no obstacles under the target area and wind flow is not blocked, resulting in a higher average wind speed.

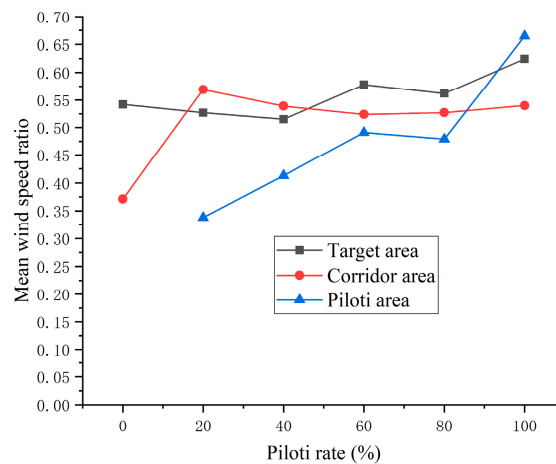


**Figure 12.** Variation of mean wind speed ratio in the point model.

Combined with Figures 13 and 14, it can be seen that the mainstream wind direction in the target area is countercurrent wind. The average wind speed ratio of the target area does not increase with the increase in the piloti rate of the building, and even slightly decreases when the piloti rate is 20% and 40%. This is because there is an opening at the bottom, resulting in the increased wind speed of the downstream wind is greater than that of the upstream wind. When the piloti rate is 60%, the increase is due to the further increase of the bottom opening, which leads to a larger increase in the upstream wind speed than the downstream wind speed.

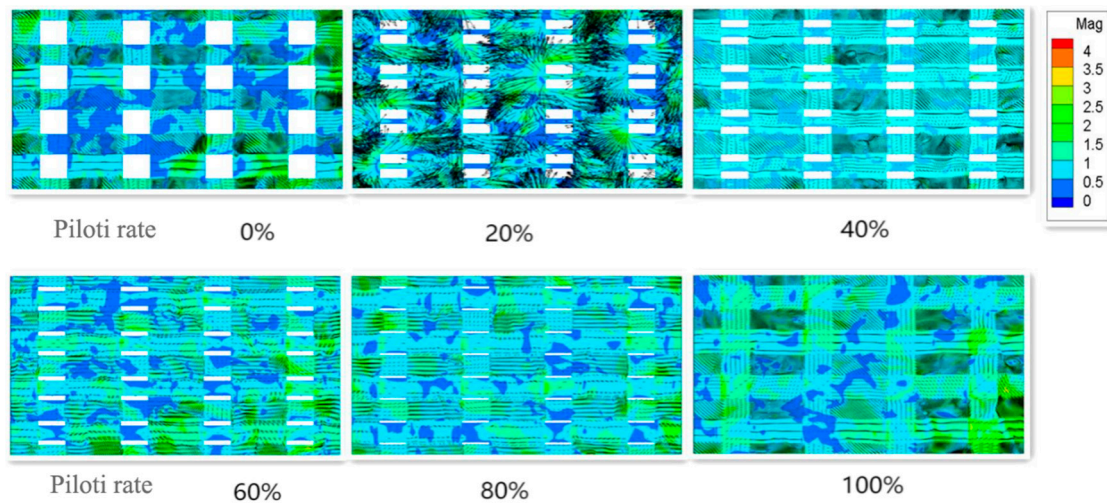


Figure 13. Vector diagram of the target area.

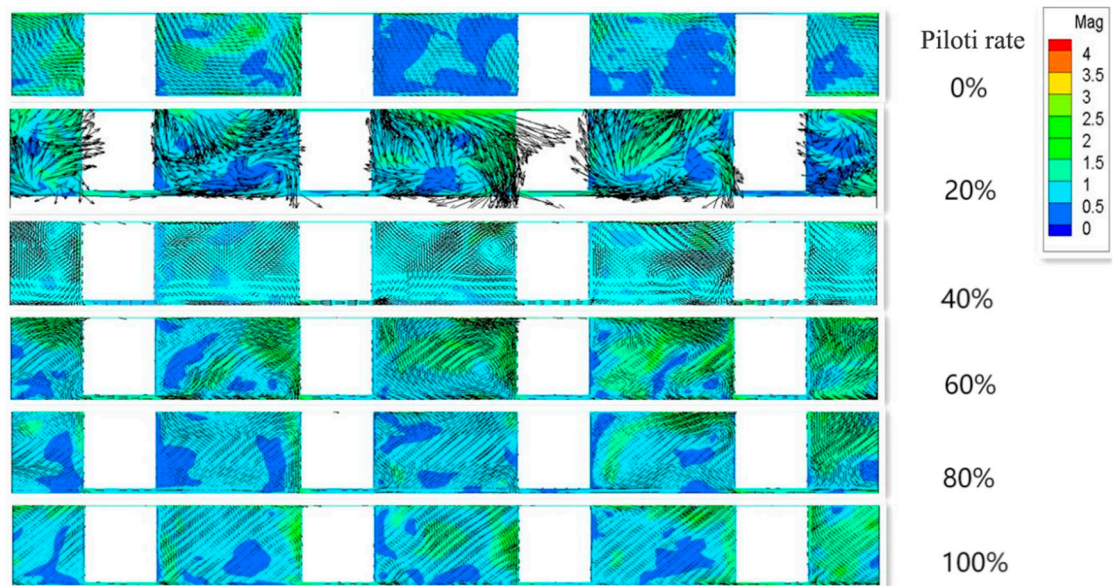
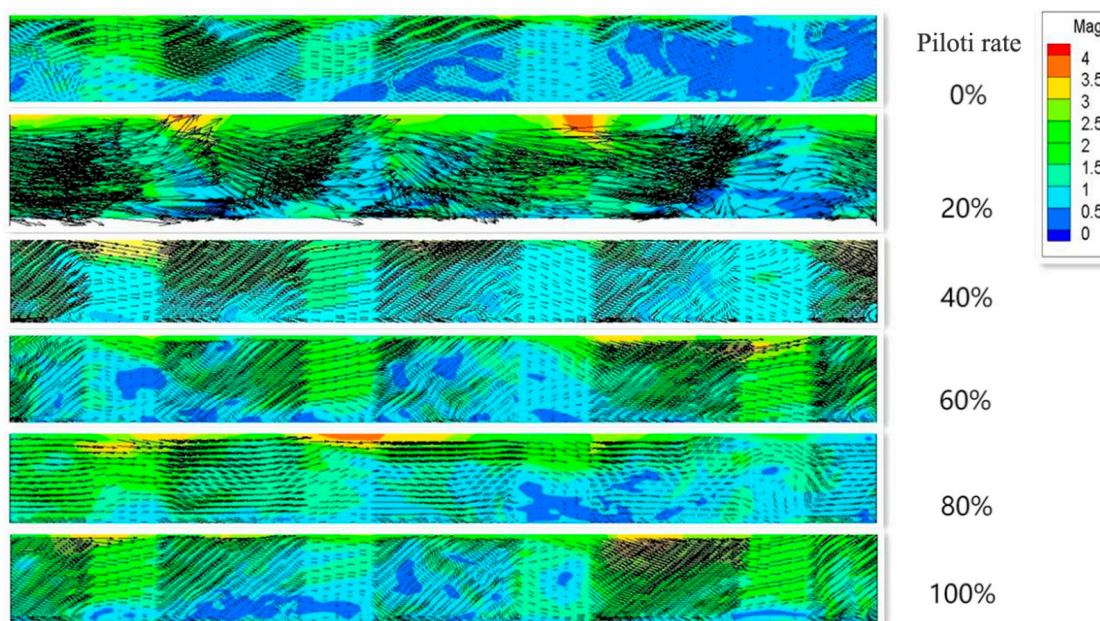


Figure 14. Vector diagram of the target area of Section 1 (Point model).

#### 4.2.2. The Effects of Piloti Design on the Wind Speed at the Pedestrian Level of the Aisle in the Target Area

It can be seen from Figure 12 that the average wind speed ratio of the corridor in the target area is the minimum under the condition of no piloti, reaches the maximum when the piloti rate is 20%, and then begins to fluctuate gently, but the fluctuation is small. Combined with Figure 15, the main wind direction of the target area is still countercurrent. This shows that, for point layout, building piloti on the first floor can greatly improve the wind speed of the middle corridor.



**Figure 15.** Vector diagram of the target area of Section 2 (Point model).

#### 4.2.3. The Effects of Piloti Design on Wind Speed of the Pedestrian Layer in the Piloti Area

As shown in Figure 12, the average wind speed ratio at a height of 1.5 m inside the piloti space presents a trend of gradual increase. It can be concluded that for the point model, with the increase in piloti rate, the average wind speed of pedestrian floors in the piloti area also increases gradually. When the piloti ratio was 60% to 80%, the average wind speed ratio decreased slightly, which may be because at a 60% piloti ratio, the average wind speed of downstream wind and countercurrent wind increased by the same amplitude, so the average wind speed did not change much. When the piloti ratio is 100%, the sudden rise in the average wind speed ratio is because there is no blockage at the bottom, so the average wind speed ratio increases.

#### 4.2.4. The Effects of Piloti Design on Pedestrian Layer Wind Comfort in Target Area

The target area of the study was sampled every 0.5 m, and 263,906, 276,593, 288,305, 300,017, 311,729, and 323,441 points were selected for the piloti rate ranging from 0% to 100%.

It can be seen from Figure 16 that in the target area, the comfortable wind ratio presents an overall upward trend with the increase in piloti rate. When the piloti rate is 100%, the comfortable wind ratio reaches its maximum.

However, when the piloti ratio was 40%, the comfortable wind ratio showed a decreasing trend compared with 20%. Combined with Figure 12, it can be seen that for the layout with a 40% piloti ratio, its average wind speed ratio in the target area is the smallest among all point models. This is due to the increase in the speed of the countercurrent wind, which leads to a decrease in the overall wind speed. Therefore, when the piloti ratio is 40%, the comfortable wind ratio decreases.

For the point model, the proportion of comfortable wind is highest when the piloti ratio is 100%. However, when the piloti rate is 100%, it is impossible to achieve, and when the piloti rate is 80%, the comfortable wind ratio is only 1.23% smaller than when the piloti rate is 100%. Therefore, it is also appropriate to choose a slightly smaller piloti rate.

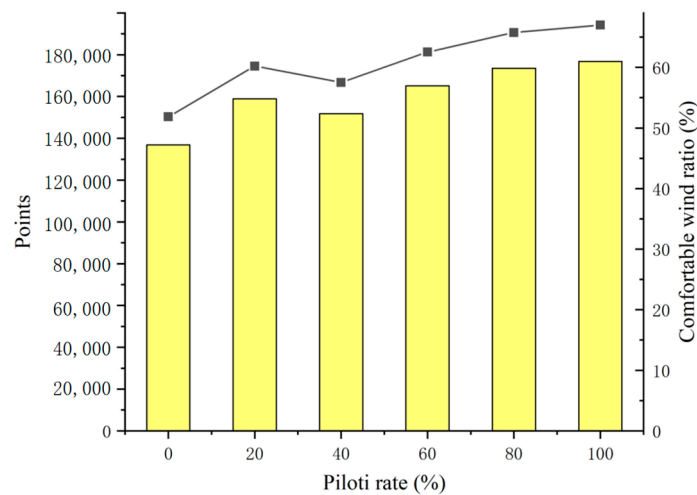
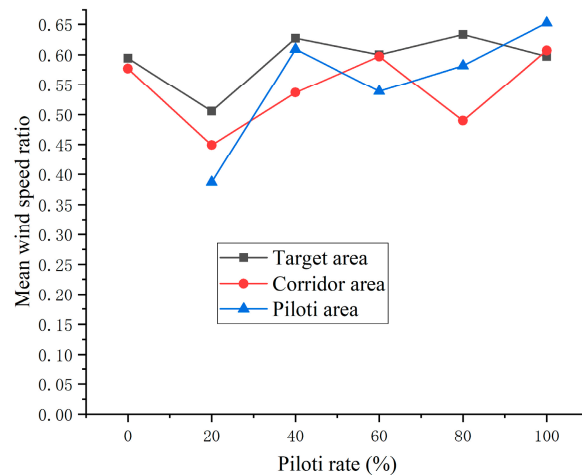


**Figure 16.** The changing pattern of a comfortable wind ratio under different piloti rates (Point model).

#### 4.3. The Effects of Piloti Design in the Enclosed Group

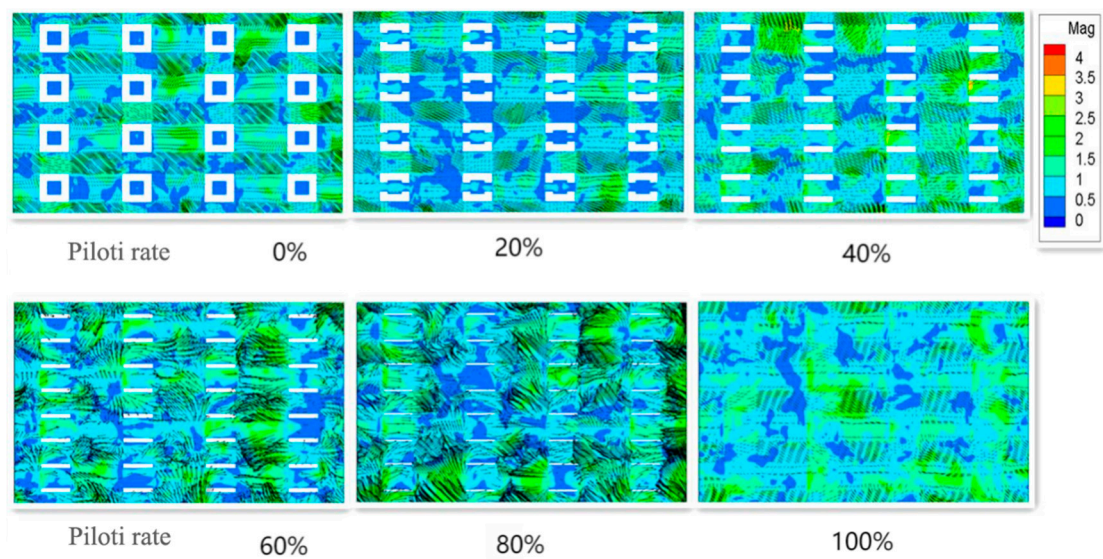
##### 4.3.1. The Effects of Piloti Design on Pedestrian Layer Wind Speed in the Target Area

Figure 17 shows that the average wind speed of pedestrian floors in the target area decreases first and then gradually flattens. This is due to the change in the building piloti rate. However, it fluctuates slightly when it is flat, and the difference in average wind speed ratio between different piloti rates is less than 0.035. This indicates that for the enclosed model, the building piloti rate has little influence on the average wind speed of pedestrian floors in the target area. Even when the piloti rate is 20%, this arrangement is not conducive to the average wind speed of the pedestrian layer in the target area.



**Figure 17.** Variation of mean wind speed ratio in the enclosed model.

According to Figures 18 and 19, the mainstream wind speed in the target area is counter-current wind. When the piloti rate is 20%, the decrease of the average wind speed is because the wind direction is partly upward, which leads to the decrease of the average wind speed in the target area. When the piloti ratio is 100%, it is lower than when it is 40%, 60%, and 80%, which is also because part of the wind direction is upward.



**Figure 18.** Vector diagram of the target area of the pedestrian layer.

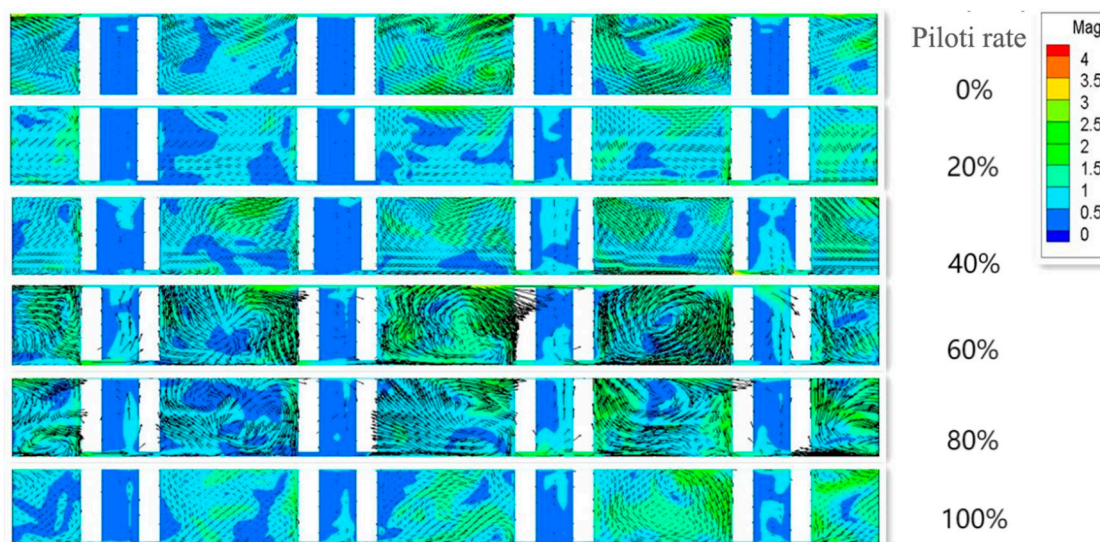


**Figure 19.** Vector diagram of the target area of Section 1 (Enclosed model).

#### 4.3.2. The Effects of Piloti Design on the Wind Speed at the Pedestrian Level of the Aisle in the Target Area

As shown in Figure 17, the average wind speed ratio of the pedestrian floor in the middle aisle of the target area shows a trend of fluctuation, and the fluctuation range is large. The maximum average wind speed ratio of the middle passage at a height of 1.5 m in the target area is 100%, which is 0.607.

When the piloti ratio is 20%, the average wind speed ratio is the lowest. At the same time, according to Figure 20, the wind flows upward and the wind speed ratio decreases because of the low piloti rate. The average wind speed ratio of the target area is the lowest when the piloti ratio is 20%.



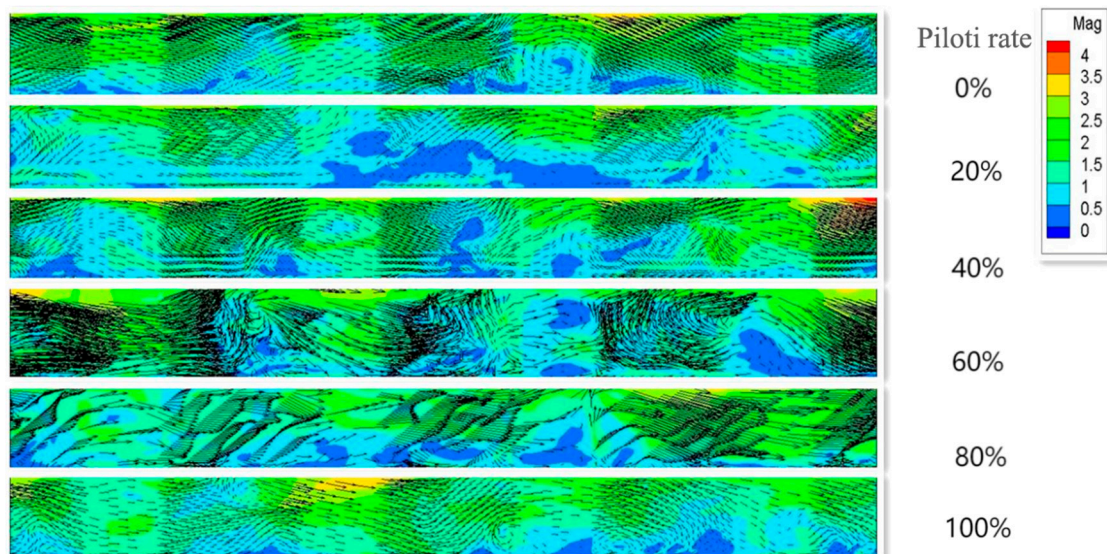


**Figure 20.** Vector diagram of the target area of Section 2 (Enclosed model).

#### 4.3.3. The Effects of Piloti Design on Wind Speed of the Pedestrian Layer in the Piloti Area

It can be seen from Figure 17 that, with the continuous increase of piloti rate, the average wind speed ratio at the height of 1.5 m in the piloti space presents an overall trend of increase. When the piloti ratio is 100%, the average wind speed ratio reaches its maximum, which is 0.652. Compared with the piloti rate of 20%, there is a great improvement.

#### 4.3.4. The Effects of Piloti Design on Pedestrian Layer Wind Comfort in the Target Area

The target area of the study was sampled every 0.5 m, and 285,985, 298,753, 312,259, 325,921, 336,961, and 348,001 points were selected for the piloti rate ranging from 0% to 100%.

It can be seen from Figure 21 that for the enclosed model, the increase in piloti rate has a certain effect on improving wind comfort in the target area of the enclosed layout, but the effect is small. Even if the piloti rate is not set correctly, it may reduce outdoor comfort.

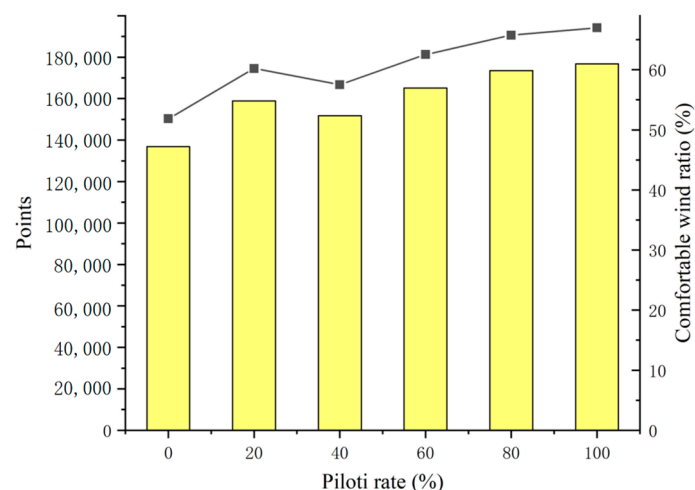


**Figure 21.** The changing pattern of a comfortable wind ratio under different piloti rates (Enclosed model).

When the piloti ratio is 20%, the comfortable wind ratio is the lowest. In combination with the vector diagram, this is due to the double effect of the side-current wind and a large part of the wind flowing upwards. Because of these two factors, when the piloti rate is 20%, the overall average wind speed ratio is smaller, which leads to a smaller comfortable wind ratio in the target area.

When the piloti ratio is 60%, the comfortable wind ratio is 65.3%. Compared with no piloti, the improvement range is 2.41%. This is a significant improvement over the 20% reduction in piloti rates and the less than 1% improvement in piloti rates of 40%, 80%, and 100%.

Therefore, it can be concluded that for the enclosed model, outdoor pedestrian wind comfort reaches its maximum when the piloti rate is 60%.

#### 4.4. Comparisons between Different Building Configurations

The piloti setting has little influence on the overall wind speed in the target area, and even an inappropriate piloti rate setting may reduce the overall average wind speed in the target area. For the determinant layout, with the increase in piloti rate, the average wind speed of pedestrian height in the target area is adversely affected. For point and enclosed layouts, setting the correct piloti rate can improve the overall mean wind speed of the area, requiring the piloti rate to be greater than 40%.

For point layouts, the piloti setting can greatly improve the average wind speed of the center aisle. This is not the case with determinant and enclosing layouts. For the determinant layout, the piloti setting reduces the average wind speed of the center aisle. The enclosed layout is the same, but when the piloti ratio is 60%, the average wind speed in the corridor is slightly increased.

At the same time, with the increase in piloti rate, the average piloti space wind speed of the three building layouts increases accordingly. This indicates that the greater the piloti ratio, the greater the wind speed inside the piloti space.

When there is no piloti condition, the determinant comfortable wind ratio is 59.14%. The point comfortable wind ratio is 51.84%; the enclosed comfortable wind ratio is 62.89%. The enclosed building layout is better than the other two kinds of building layout when there is no piloti. The point layout had the worst wind comfort ratio and was much lower than the other two layouts. For the determinant model, the point model, and the enclosed model, the maximum comfortable wind ratios in the target area are 68.44%, 66.99%, and 65.3% when the piloti ratio is 80%, 100%, and 60%, respectively. The wind comfort ratio is highest when the row layout and piloti ratio are both at 80%. Compared with the no piloti condition, the piloti rate of determinant, point, and enclosure models are improved by 9.3%, 15.15%, and 2.41%, respectively. The comfortable wind ratio is most obvious in the ground-floor piloti point-to-point layout. For the enclosed model, the improvement effect of the bottom frame is poor.

## 5. Conclusions

This paper mainly studies the influence of different piloti ratios on outdoor wind comfort for three typical building layouts. A total of six different piloti rates were set: 0%, 20%, 40%, 60%, 80%, and 100%. Three common residential building layouts in Wuhan, China were selected as the research objects, which are determinant type, point type, and enclosed type. There were 18 sets of models. The average wind speed was compared among the target area, the middle corridor of the building, and the pedestrian layer of the building's piloti space. The outdoor wind comfort was analyzed by the comfortable wind ratio.

The results show that: (1) The piloti setting has little influence on the overall wind speed in the target area, and even an inappropriate piloti rate setting may reduce the overall mean wind speed in the target area. (2) For point layout, the piloti setting can improve the average wind speed in the middle passage. However, for the determinant and enclosure layout, the average wind speed in the corridor area will be reduced. (3) With the increase in piloti rate, the average wind speed of the piloti area can be improved. (4) A comprehensive comparison of the three building layouts shows that the comfortable wind ratio of the determinant layout is the highest when the piloti ratio is 80%.

The results of this study can provide architects and urban planners with reference for piloti and urban layout design. The reasonable piloti rate setting can significantly improve outdoor wind comfort as well as outdoor pedestrian wind comfort in densely built cities.

**Author Contributions:** Methodology, Q.D.; software, X.S.; validation, Y.H., C.H. and G.L.; formal analysis, Z.R.; resources, Q.D.; data curation, Y.H.; writing—original draft preparation, Y.H.; writing—review and editing, Y.H.; supervision, Q.D. and Q.T.; funding acquisition, Q.D., X.S. and Q.T. All authors have read and agreed to the published version of the manuscript.

**Funding:** This research was funded by the Hainan Province Science and Technology Special Fund, ZDKJ2021024 and the Sanya Science and Education Innovation Park of Wuhan University of Technology, 2021KF0002 and 2021KF0004.

**Data Availability Statement:** Not applicable.

**Acknowledgments:** This research is supported by Luneng Group Co., Ltd.’s “Research Project on Relevant Upgrade Technology Solutions to Respond to the New Green Building Evaluation Standards”.

**Conflicts of Interest:** The authors declare no conflict of interest.

## References

1. Wang, W.; Wang, X.; Ng, E. The coupled effect of mechanical and thermal conditions on pedestrian-level ventilation in high-rise urban scenarios. *Build. Environ.* **2021**, *191*, 107586. [[CrossRef](#)]
2. Zou, J.; Yu, Y.; Liu, J.; Niu, J.; Chauhan, K.; Lei, C. Field measurement of the urban pedestrian level wind turbulence. *Build. Environ.* **2021**, *194*, 107713. [[CrossRef](#)]
3. Zou, J.; Liu, J.; Niu, J.; Yu, Y.; Lei, C. Convective heat loss from computational thermal manikin subject to outdoor wind environments. *Build. Environ.* **2021**, *188*, 107469. [[CrossRef](#)]
4. Cao, S.-H.; Ming, P.-P.; Zhao, X. Fuzzy comprehensive evaluation of human thermal comfort in simulating natural wind environment. *Build. Environ.* **2021**, *188*, 107447. [[CrossRef](#)]
5. Tominaga, Y.; Shirzadi, M. Wind tunnel measurement of three-dimensional turbulent flow structures around a building group: Impact of high-rise buildings on pedestrian wind environment. *Build. Environ.* **2021**, *206*, 108389. [[CrossRef](#)]
6. Kikumoto, H.; Choi, W.; Ooka, R. Development of probabilistic assessment framework for pedestrian wind environment using Bayesian technique. *Build. Environ.* **2021**, *187*, 107419. [[CrossRef](#)]
7. Du, Y.; Mak, C.M.; Ai, Z. Modelling of pedestrian level wind environment on a high-quality mesh: A case study for the HKPolyU campus. *Environ. Model. Softw.* **2018**, *103*, 105–119. [[CrossRef](#)]
8. Wu, Y.; Zhan, Q.; Quan, S.J. Improving local pedestrian-level wind environment based on probabilistic assessment using Gaussian process regression. *Build. Environ.* **2021**, *205*, 108172. [[CrossRef](#)]
9. Weerasuriya, A.U.; Zhang, X.; Lu, B.; Tse, K.T.; Liu, C.H. A Gaussian Process-Based emulator for modeling pedestrian-level wind field. *Build. Environ.* **2021**, *188*, 107500. [[CrossRef](#)]
10. Ricci, A.; Guasco, M.; Caboni, F.; Orlanno, M.; Giachetta, A.; Repetto, M.P. Impact of surrounding environments and vegetation on wind comfort assessment of a new tower with vertical green park. *Build. Environ.* **2022**, *207*, 108409. [[CrossRef](#)]
11. Kabošová, L.; Chronis, A.; Galanos, T.; Kmet', S.; Katunský, D. Shape optimization during design for improving outdoor wind comfort and solar radiation in cities. *Build. Environ.* **2022**, *226*, 109668. [[CrossRef](#)]
12. Gao, H.; Liu, J.; Lin, P.; Li, C.; Xiao, Y.; Hu, G. Pedestrian level wind flow field of elevated tall buildings with dense tandem arrangement. *Build. Environ.* **2022**, *226*, 109745. [[CrossRef](#)]
13. Hu, H.; Chen, Q.; Qian, Q.; Zhou, X.; Chen, Y.; Cai, Y. Field investigation for ambient wind speed and direction effects exposure of cyclists to PM<sub>2.5</sub> and PM<sub>10</sub> in urban street environments. *Build. Environ.* **2022**, *223*, 109483. [[CrossRef](#)]
14. Takebayashi, H. Effects of air temperature, humidity, and wind velocity distribution on indoor cooling load and outdoor human thermal environment at urban scale. *Energy Build.* **2022**, *257*, 111792. [[CrossRef](#)]
15. Yang, Q.; Xu, X.; Lin, Q.; Tamura, Y. Generic models for predicting pedestrian-level wind around isolated square-section high-rise buildings. *J. Wind Eng. Ind. Aerodyn.* **2022**, *220*, 104842. [[CrossRef](#)]
16. Shirzadi, M.; Tominaga, Y. Multi-fidelity shape optimization methodology for pedestrian-level wind environment. *Build. Environ.* **2021**, *204*, 108076. [[CrossRef](#)]
17. Cui, D.; Hu, G.; Ai, Z.; Du, Y.; Mak, C.M.; Kwok, K. Particle image velocimetry measurement and CFD simulation of pedestrian level wind environment around U-type street canyon. *Build. Environ.* **2019**, *154*, 239–251. [[CrossRef](#)]
18. Weerasuriya, A.U.; Tse, K.T.; Zhang, X.; Li, S.W. A wind tunnel study of effects of twisted wind flows on the pedestrian-level wind field in an urban environment. *Build. Environ.* **2018**, *128*, 225–235. [[CrossRef](#)]
19. He, Y.; Liu, Z.; Ng, E. Parametrization of irregularity of urban morphologies for designing better pedestrian wind environment in high-density cities—A wind tunnel study. *Build. Environ.* **2022**, *226*, 109692. [[CrossRef](#)]
20. Ikegaya, N.; Kawaminami, T.; Okaze, T.; Hagishima, A. Evaluation of exceeding wind speed at a pedestrian level around a 1:1:2 isolated block model. *J. Wind Eng. Ind. Aerodyn.* **2020**, *201*, 104193. [[CrossRef](#)]
21. Du, Y.; Mak, C.M.; Li, Y. Application of a multi-variable optimization method to determine lift-up design for optimum wind comfort. *Build. Environ.* **2018**, *131*, 242–254. [[CrossRef](#)]
22. Li, J.; Wang, W.; Jin, H.; Li, Y.; Bu, N. Thermal responses of people exhibiting high metabolic rates when exercising in pilot spaces in hot and humid areas. *J. Build. Eng.* **2022**, *48*, 103930. [[CrossRef](#)]

23. Du, Y.; Mak, C.M.; Liu, J.; Xia, Q.; Niu, J.; Kwok, K.C.S. Effects of lift-up design on pedestrian level wind comfort in different building configurations under three wind directions. *Build. Environ.* **2017**, *117*, 84–99. [[CrossRef](#)]
24. Huang, T.; Niu, J.; Xie, Y.; Li, J.; Mak, C.M. Assessment of “lift-up” design’s impact on thermal perceptions in the transition process from indoor to outdoor. *Sustain. Cities Soc.* **2020**, *56*, 102081. [[CrossRef](#)]
25. Sha, C.; Wang, X.; Lin, Y.; Fan, Y.; Chen, X.; Hang, J. The impact of urban open space and ‘lift-up’ building design on building intake fraction and daily pollutant exposure in idealized urban models. *Sci. Total Environ.* **2018**, *633*, 1314–1328. [[CrossRef](#)] [[PubMed](#)]
26. Tse, K.T.; Zhang, X.; Weerasuriya, A.U.; Li, S.W.; Kwok, K.C.S.; Mak, C.M.; Niu, J. Adopting ‘lift-up’ building design to improve the surrounding pedestrian-level wind environment. *Build. Environ.* **2017**, *117*, 154–165. [[CrossRef](#)]
27. Chen, L.; Mak, C.M. Integrated impacts of building height and upstream building on pedestrian comfort around ideal lift-up buildings in a weak wind environment. *Build. Environ.* **2021**, *200*, 107963. [[CrossRef](#)]
28. Smagorinsky, J. General Circulation Experiments with the Primitive Equations. *Mon. Weather Rev.* **1963**, *91*, 99–164. [[CrossRef](#)]
29. Murakami, S.; Mochida, A. On turbulent vortex shedding flow past 2D square cylinder predicted by CFD. *J. Wind Eng. Ind. Aerodyn.* **1995**, *54–55*, 191–211. [[CrossRef](#)]
30. Yu, D.; Kareem, A. Numerical simulation of flow around rectangular prism. *J. Wind Eng. Ind. Aerodyn.* **1997**, *67–68*, 195–208. [[CrossRef](#)]
31. Shah, K.B.; Ferziger, J.H. A fluid mechanics view of wind engineering: Large eddy simulation of flow past a cubic obstacle. *J. Wind Eng. Ind. Aerodyn.* **1997**, *67–68*, 211–224. [[CrossRef](#)]
32. Panneer Selvam, R. Computation of pressures on Texas Tech University building using large eddy simulation. *J. Wind Eng. Ind. Aerodyn.* **1997**, *67–68*, 647–657. [[CrossRef](#)]
33. Kravchenko, A.G.; Moin, P. Numerical studies of flow over a circular cylinder at  $Re_D = 3900$ . *Phys. Fluids* **2000**, *12*, 403. [[CrossRef](#)]
34. Tutar, M.; Oguz, G. Large eddy simulation of wind flow around parallel buildings with varying configurations. *Fluid Dyn. Res.* **2002**, *31*, 289–315. [[CrossRef](#)]
35. Lim, H.C.; Thomas, T.G.; Castro, I.P. Flow around a cube in a turbulent boundary layer: LES and experiment. *J. Wind Eng. Ind. Aerodyn.* **2009**, *97*, 96–109. [[CrossRef](#)]
36. Murakami, S.; Morikawa, Y. Criteria for assessing wind-induced discomfort considering temperature effect. *J. Archit. Plan. Environ. Eng.* **1985**, *358*, 9–17.
37. Tominaga, Y.; Mochida, A.; Yoshie, R.; Kataoka, H.; Nozu, T.; Yoshikawa, M.; Shirasawa, T. AIJ guidelines for practical applications of CFD to pedestrian wind environment around buildings. *J. Wind Eng. Ind. Aerodyn.* **2008**, *96*, 1749–1761. [[CrossRef](#)]
38. Blocken, B.; Gualtieri, C. Ten iterative steps for model development and evaluation applied to Computational Fluid Dynamics for Environmental Fluid Mechanics. *Environ. Model. Softw.* **2012**, *33*, 1–22. [[CrossRef](#)]
39. Nation Meteorological Information Center. *China’s Special Meteorological Data Set for Thermal Environment Analysis*; China Architecture and Building Press: Beijing, China, 2005.

**Disclaimer/Publisher’s Note:** The statements, opinions and data contained in all publications are solely those of the individual author(s) and contributor(s) and not of MDPI and/or the editor(s). MDPI and/or the editor(s) disclaim responsibility for any injury to people or property resulting from any ideas, methods, instructions or products referred to in the content.